Applied Rheology | DOI: 10.3933/APPLRHEOL-26-14289 | WWW.APPLIEDRHEOLOGY.ORG

Exploring the Nonlinear Viscoelasticity of a High Viscosity Silicone Oil with LAOS

Z. Kőkuti[1,2], L. Völker-Pop[3], M. Brandstätter[4], J. Kokavecz[1], P. Ailer[5], L. Palkovics[5], G. Szabó[1], A. Czirják[1,2]*

[1]Institute of Engineering and Materials Science, University of Szeged, Tisza L. krt. 103, 6720 Szeged, Hungary
[2]Department of Theoretical Physics, University of Szeged, Tisza L. krt. 84-86, 6720 Szeged, Hungary
[3]Anton Paar Germany GmbH, Helmuth-Hirth-Str. 6, 73760 Ostfildern, Germany
[4]Anton Paar GmbH, Anton-Paar-Str. 20, 8054 Graz, Austria
[5]Department of Vehicle Technology, Kecskemét College, Izsáki út 10, 6000 Kecskemét, Hungary

* Corresponding author: czirjak@physx.u-szeged.hu

Received: 21.7.2015, Final version: 2.11.2015

Abstract:
Measurements and modeling of the nonlinear viscoelastic properties of a high viscosity silicone oil (polydimethylsiloxane, PDMS) are reported. LAOS test were performed with a high precision rotational rheometer to probe the nonlinear response. The measurements show that the material can be safely considered linear below strain amplitude 1. The viscous Lissajous-Bodwitch curves indicate intracycle shear thinning, whereas the elastic Lissajous-Bodwitch curves indicate intracycle strain stiffening in the nonlinear regime. Secondary loops in some of the measured viscous stress curves are attributed to a non-sinusoidal shear rate signal. A multi-element White-Metzner model is used as a constitutive equation, which accurately describes the LAOS data in all measured cases. Based on the extension of the measured data by simulations, nonlinear properties are analyzed both for the elastic and for the viscous part. It is observed that the nonlinearity considerably increases the weight of the higher harmonics in the shear stress signal. It is predicted that the viscous nonlinearity has a maximum around 50 rad/s angular frequency, and that the elastic nonlinearity becomes nearly independent of the angular frequency above 30 rad/s.

Key words:
LAOS, PDMS, nonlinear viscoelasticity, White-Metzner model, intracycle shear thinning

1 INTRODUCTION

Silicone oils are important viscoelastic fluids, with a broad range of use from fundamental science to industrial applications [1–12]. Linear viscoelastic properties of silicone oils, usually with rather low zero-shear viscosity, have been studied in a number of papers, as well as their shear thinning behavior [2, 13]. High viscosity silicon oils were investigated only in a few cases [14–17], including high-frequency measurements [18, 19]. If the deformations of the silicone oil are large enough, nonlinear viscoelastic properties control its material response. This is of increasing importance, both in polymer research and in engineering applications. Amplitude sweep test were already published in our previous work [19], but a more extensive analysis has not been done yet on the nonlinear viscoelasticity of high viscosity silicone oils, to the best of our knowledge. Now we extend our former investigations and report on LAOS measurement with high viscosity PDMS to explore deeper the nonlinear viscoelastic properties. We use the silicone oil AK 1.000.000 from Wacker as the test material, since the viscoelastic properties of this silicone oil well represent that of a whole range of silicone oils with different zero-shear viscosities. Large amplitude oscillatory shear (LAOS) is a commonly used method to characterize the nonlinear viscoelastic properties of the materials [20].

The most common method to quantify LAOS tests is Fourier transform (FT) rheology [21]. For a sinusoidal strain input, the stress response could be described by a Fourier series [22]. Only odd harmonics are included in these series because the stress signal is assumed to be of odd symmetry with respect to directionality of shear strain or shear rate, i.e., the material response is unchanged if the coordinate system is reversed [23]. Another way to quantify nonlinear viscoelasticity in LAOS is the stress decomposition (SD) technique. Here the stress response is decomposed to elastic and viscous stresses. The elastic stress should exhibit odd sym-

metry to shear strain and the viscous stress should exhibit even symmetry to shear strain (odd symmetry to shear rate) [24]. Our paper is organized as follows: First we review the most important features and quantities of LAOS analysis performed on a nonlinear viscoelastic fluid. Then we present our LAOS test results and analyze them, including the limitations of the measurements performed. Next, we test our nonlinear viscoelastic constitutive equations using the raw measured data, and based on this we extend our LAOS analysis with the help of simulations. Finally, we make some conclusion.

2 REVIEW OF LAOS-RELATED NONLINEAR VISCOELASTIC QUANTITIES

A basic test to explore the nonlinear viscoelastic regime is amplitude sweep, when only the fundamental harmonic component of the shear stress is computed. Much more information about nonlinear viscoelasticity can be obtained using Large Amplitude Oscillatory Shear (LAOS) tests, which is a well-defined method to probe the nonlinear properties of the sample. A sinusoidal strain of the form $\gamma(t) = \gamma_o \sin(\omega t)$ is applied to the material and the measured raw shear stress signal is analyzed. Scanning both the strain amplitude and the oscillation frequency, detailed characterization of the material's nonlinear viscoelastic properties can be obtained.

In the past, several methods have been proposed to analyze the non-linear data obtained from LAOS experiments. For instance, the raw stress signal $\sigma(t)$ can be graphically visualized as a function of strain $\gamma(t)$ or strain rate $\dot{\gamma}(t)$ resulting respectively in elastic or viscous Lissajous-Bowditch plots [25–29]. Such curves qualitatively show evidence of non-linearities, as the shape of the closed loops starts to deviate from an ellipsoidal shape. The characterization of nonlinear viscoelasticity based on LAOS measurements uses several different quantities. In this paper we use both the FT-rheology and the Ewoldt quantities which can be considered standard by now. The output stress signal at steady-state can be represented by a Fourier series of odd harmonics [20].

$$\sigma(t,\omega,\gamma_o) = \gamma_o \sum_{n:odd} \left(G'_n(\omega,\gamma_o) \sin(n\omega t) + G''_n(\omega,\gamma_o) \cos(n\omega t) \right) \quad (1)$$

The FT-rheology methodology can be applied to various complex fluids, for example, emulsions [30], suspensions [31], dilute or concentrated polymer solutions and poly-

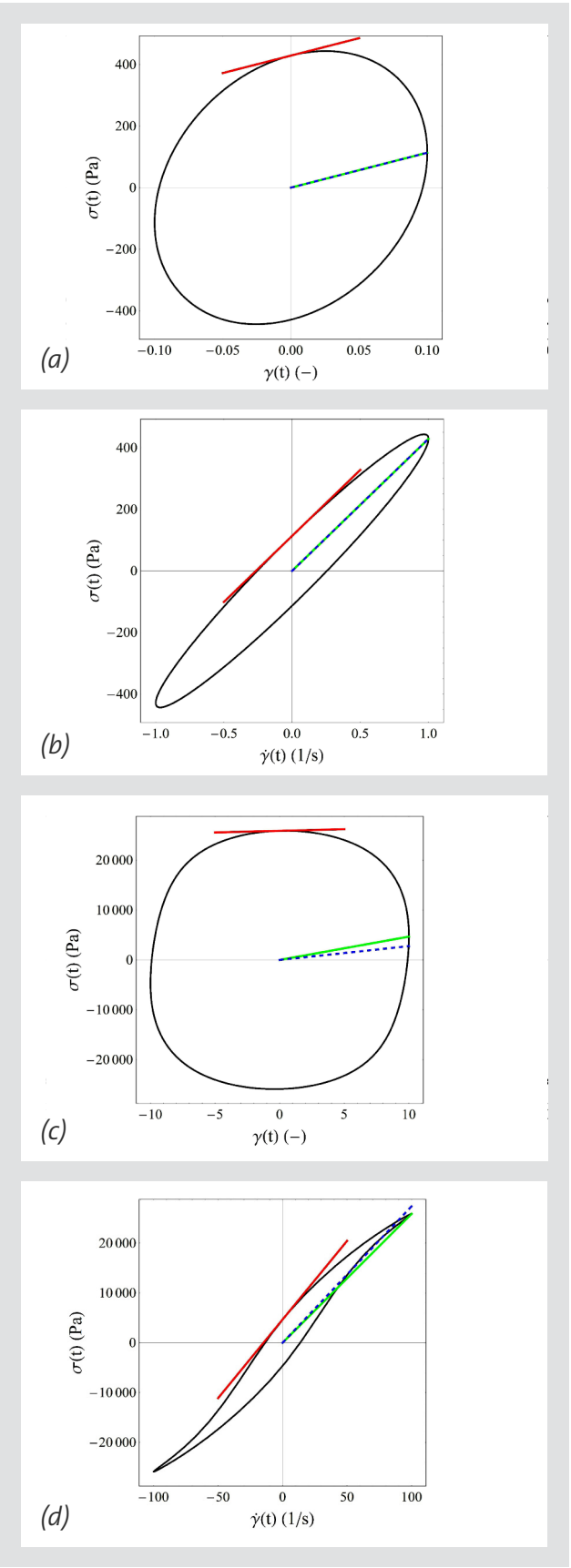

Figure 1: Graphical interpretation of the minimum (red) and large quantities (green), as defined in Equations 2 and 3, shown for data obtained with silicon oil sample AK 1.000.000 (Wacker). The first harmonic moduli (blue) are also shown for comparison. Plots (a) and (b) present linear viscoelastic response (ω = 10 rad/s, γ_o = 0.1), whereas plots (c) and (d) present nonlinear viscoelastic behavior (ω = 10 rad/s, γ_o = 10).

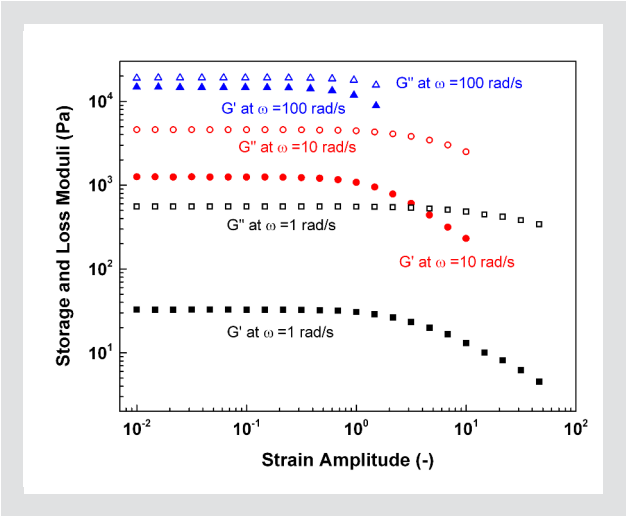

Figure 2: Amplitude sweep data, measured at 60°C temperature and at the indicated angular frequencies, show strain thinning behavior of the silicone oil AK 1.000.000. Full (open) symbols represent the storage (loss) modulus.

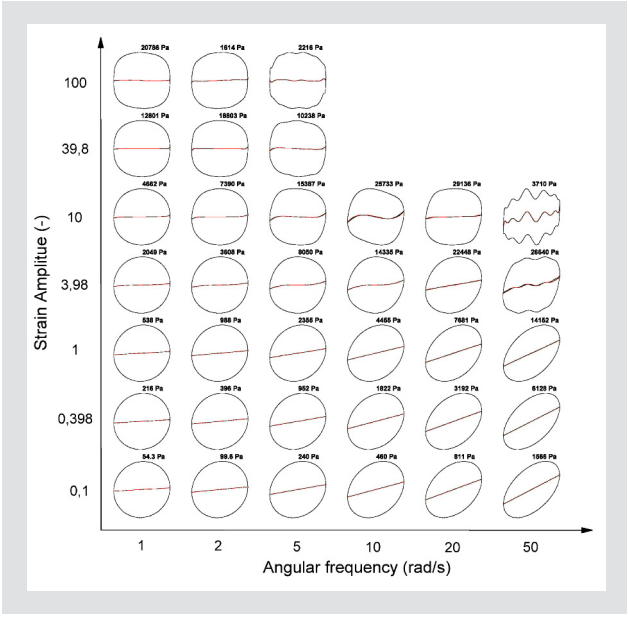

Figure 3: LAOS data for the silicon oil shown as normalized elastic Lissajous-Bodwitch curves at selected strain amplitudes. We use black lines for the raw shear stress, whereas red lines for the elastic shear stress. The maximum shear stress is also indicated above each curve.

mer melts [32–37]. To represent the elastic and viscous behavior of the material, Ewoldt et al. defined two new physically meaningful elastic and viscous properties [38]:

$$G'_M \equiv \left.\frac{d\sigma}{d\gamma}\right|_{\gamma=o}, \qquad G'_L \equiv \left.\frac{\sigma}{\gamma}\right|_{\gamma=\pm\gamma_o} \tag{2}$$

$$\eta'_M \equiv \left.\frac{d\sigma}{d\dot{\gamma}}\right|_{\dot{\gamma}=o}, \qquad \eta'_L \equiv \left.\frac{\sigma}{\dot{\gamma}}\right|_{\dot{\gamma}=\pm\dot{\gamma}_o} \tag{3}$$

where G'_M is the minimum strain modulus at γ = 0 and G'_L is the large strain modulus at the maximum imposed strain. Analogously, η'_M is the minimum rate dynamic viscosity at $\dot{\gamma}(t)$ = 0 and η'_L is the large rate dynamic viscosity at the maximum imposed shear rate. We present the graphical interpretation of these parameters with the help of the elastic and viscous Lissajous-Bodwitch curves for our silicon oil sample in Figure 1. The black loops are the raw stress signals versus the raw shear or shear rate signals. The red tangent lines show the minimum values G'_M and η'_M, the green lines show the largest values G'_L and η'_L and the dotted blue lines show the first harmonic values G'_1 and $\eta'_1 = G''_1/\omega$. In the linear regime $G'_M = G'_L = G'_1 = e_1$ and $\eta'_M = \eta'_L = \eta'_1 = v_1$ as show by Figures 1a and 1b. In the nonlinear case these parameters are different as show by Figures 1c and 1d. Note that we specify the strain with its decimal value in this paper, i.e. strain amplitude γ_o = 1 means 100 %. Ewoldt et al. define also two other parameters to characterize intracycle nonlinearities: The strain-stiffening ratio is

$$S \equiv \frac{G'_L - G'_M}{G'_L} = \frac{4e_3 + \ldots}{e_1 + e_3 + \ldots} \tag{4}$$

The S = 0 represent linear elastic response, whereas S < 0 (> 0) indicates intracycle strain stiffening (softening) [38]. The shear thickening ratio is

$$T \equiv \frac{\eta'_L - \eta'_M}{\eta'_L} = \frac{4v_3 + \ldots}{v_1 + v_3 + \ldots} \tag{5}$$

The T = 0 represent linear viscous response, whereas T < 0 (> 0) indicates intracycle shear thickening (thinning) [38]. Here we note that this formalism was extended also for LAOS with sinusoidal stress input [39].

3 RESULTS

Our previous amplitude sweep tests [19] suggest that the silicone oil AK 1.000.000 (Wacker) has strain thinning behavior in the entire measured angular frequency range: both the storage and the loss moduli decrease if we increase the amplitude of the oscillation. The onset of nonlinear behavior occurs at decreasing shear amplitude values as we increase the angular frequency. Figure 2 shows this behavior at selected values of the angular frequencies. This strain thinning behavior of the silicon fluid can be explained similarly as its shear thinning behavior: when the strain amplitude is more and more increased, the polymer chains more and more align with the flow field and that is why both the loss and the storage moduli decrease [40].

To have a better insight into the nonlinear properties of the material we performed true LAOS test. Our measurements were done with an Anton Paar MCR702 rheometer. This is the latest model of the company, with

increased precision and twin motor setup. The instrument is able to measure the raw shear strain and shear stress data. To avoid the outflow of the material at high strain amplitudes we used CC10 (concentric cylinder measuring head with 10 mm inner diameter) geometry. For the data analysis we used the new RheoCompass software. The strain controlled LAOS test were measured at frequencies of ω = 1, 2, 5, 10, 20, 50 rad/s and at a strain amplitude range of γ_o from 0.1 to 100 with 6 points per decade and at constant temperature of T = 60°C. We used a new silicone oil sample for each measurement case.

To analyze the raw stress signal we use Lissajous-Bodwitch curves, which visually show the intracycle viscoelastic response: the elastic Lissajous-Bodwitch curve (raw shear stress data versus raw strain data) and the viscous Lissajous-Bodwitch curve (raw shear stress data versus raw shear rate data). The normalized elastic Lissajous-Bodwitch curves as a function of both frequency and strain amplitude are shown in Figure 3, while the corresponding normalized viscous Lissajous-Bodwitch curves are shown in Figure 4. In these figures we also plot the elastic σ' and viscous σ'' stresses in red,as defined by [24]:

$$\sigma'(t) \equiv \frac{\sigma(\gamma,\dot{\gamma}) - \sigma(-\gamma,\dot{\gamma})}{2} = \sum_{n:odd} G_n'(\omega,\gamma_o) sin(n\omega t) \tag{6}$$

$$\sigma''(t) \equiv \frac{\sigma(\gamma,\dot{\gamma}) - \sigma(\gamma,-\dot{\gamma})}{2} = \sum_{n:odd} G_n''(\omega,\gamma_o) cos(n\omega t) \tag{7}$$

Note, that the Fourier series decomposition contains only odd harmonic components, due to the symmetry properties of the stress signal [23]. For the decomposition we used the RheoCompass software. The values of the maximal shear stress σ_{MAX} are also shown above the curves. The Lissajous-Bodwitch curves having elliptical shape, which therefore yield straight elastic and viscous stress curves, indicate linear viscoelasticity. At small strain amplitudes, i.e. below 1, both the elastic and viscous curves show linear viscoelasticity, in full agreement with the interpretation of the amplitude sweep measurements. Nonlinearity can be observed at higher amplitudes, the magnitude of the nonlinearity depends not only on the strain amplitude but also on the frequency.

However, in some cases the maximum stress amplitudes suddenly decrease instead of increasing with the strain amplitude, see frequency and deformation pairings (ω, γ_o) of (2, 100), (5, 39.8), (5, 100), and (50, 10). Furthermore, these curves look rather distorted. These measurement cases are strongly influenced by the

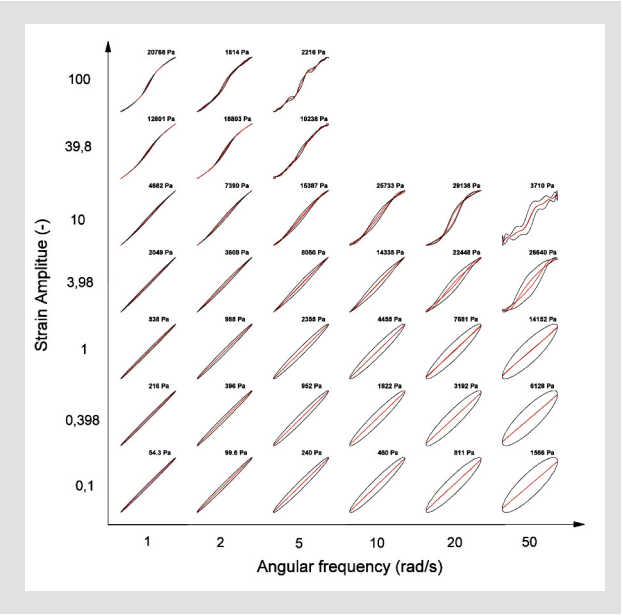

Figure 4: LAOS data for the silicon oil shown as normalized viscous Lissajous-Bodwitch curves at selected strain amplitudes. We use black lines for the raw shear stress, whereas red lines for the viscous shear stress. The maximum shear stress is also indicated above each curve.

Weissenberg-effect therefore we do not regard these data as valid measurements. In the nonlinear regime, the elastic Lissajous-Bodwitch curves show intracycle strain stiffening whereas the viscous Lissajous-Bodwitch curves show intracycle shear thinning. However, having a closer a look at the viscous curves, we see that in many cases the viscous stress curves have secondary loops. This effect occurs because the input strain signal is not a pure sinusoidal anymore in these cases. If the strain signal is not a pure sine function than the Cho decomposition is not applicable anymore. The software uses the Fourier stress decomposition and in these cases this could be deceptive. It is hard to decide whether the stress signal is nonlinear dominantly due to the material nonlinearity or due to the non-sinusoidal input strain signal.

4 DISCUSSION OF THE LAOS MEASUREMENTS

In order to check the non-sinusoidal character of the input strain signal we start out from its Fourier series decomposition:

$$\gamma(t) = \sum_n \tilde{\gamma}_n sin(n\omega t) \tag{8}$$

We check the ratio of the amplitude of the 3^{rd} harmonic component to the fundamental component

$$r_{31} \equiv \frac{\tilde{\gamma}_3}{\tilde{\gamma}_1} = \frac{\tilde{\gamma}_3}{\gamma_o}$$

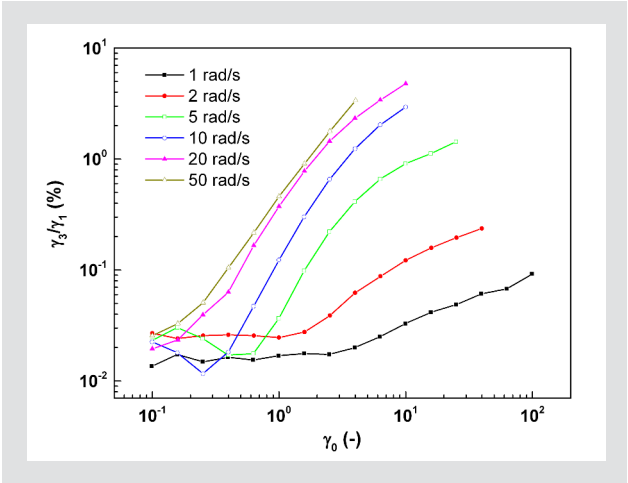

Figure 5: The ratio of the strain amplitude of the 3rd harmonic component to the fundamental component r31 as a function of the fundamental component γ_o for all the measured angular frequencies.

We plot this quantity as a function of γ_o for all the measured angular frequencies in Figure 5. Those measurement cases which were influenced by the Weissenberg-effect were not included in this analysis. As we see, r_{31} is below 5 % even at high frequencies and strain amplitudes. The higher frequency components are negligible. Thus the input strain signal itself is rather close to a pure sinusoid in good agreement with the fact that the elastic stress curves in Figure 3 do not have any secondary loops. However this is not the case for the shear rate obtained from the input strain signal. Calculating the shear rate by the derivation of Equation 8:

$$\dot{\gamma}(t)=\sum_n \tilde{\gamma}_n n\omega cos(n\omega t) \tag{9}$$

it is easy to see that the ratio of the amplitude of its n^{th} harmonic component to the fundamental component is n times larger than the analogous strain quantity. So where the strain signal still does not differ much from a single sinusoidal (r_{31} = 5 %), the shear rate signal differs considerably stronger from the pure sinusoidal ($\tilde{\dot{\gamma}}_3/\tilde{\dot{\gamma}}_1$ = 15 %). This distortion has a more pronounced effect on the viscous stress curves as shown by the secondary loops in Figure 4, since this PDMS sample is dominantly viscous in the measured frequency range. Therefore, we do not consider those measurement cases, which have secondary loops in the viscous or in the elastic stress, being suitable for the usual LAOS analysis.

However, the shear or shear-rate versus shear stress relation is still accurately measured in these cases, and it contains the nonlinear viscoelastic information about the material. Therefore, these measurement cases can be utilized as verification test cases for simulations with a nonlinear viscoelastic constitutive equation: as long as the tested constitutive equation is able to simulate the measured shear stress in the case of the non-sinusoidal shear or shear-rate, it is obvious that this constitutive equation gives reliable results

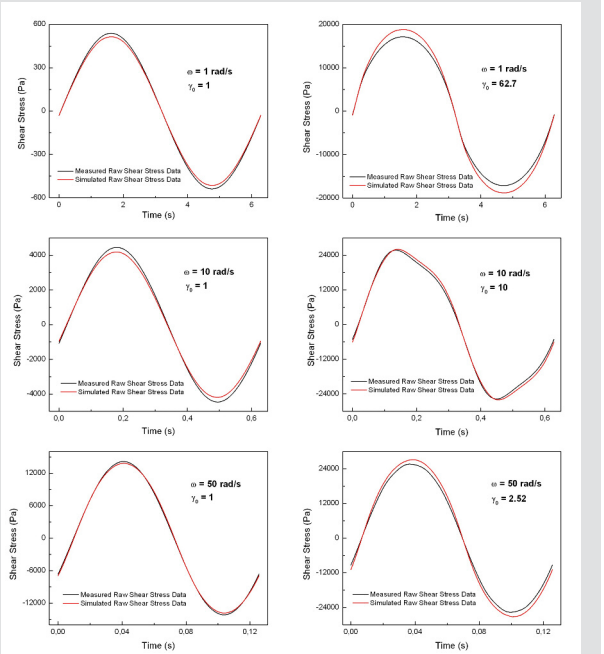

Figure 6: Comparison of simulated (red) and measured raw (black) shear stress data versus time, at several selected representative angular frequencies and amplitudes. The plot to the left belongs to the linear amplitude regime and the plot to the right represents a nonlinear case.

also for a simple sinusoidal input with the same amplitude and angular frequency. Since this latter is a simulated LAOS test, it follows that we can safely replace the measured data with simulated LAOS data in these measurement cases.

5 CONSTITUTIVE MODEL AND SIMULATIONS

We use the constitutive equation published in our earlier work [19]. This is based on a 6 element Maxwell model, which was fitted to the joined SAOS and DWS storage and loss moduli. The following equations define our nonlinear White-Metzner-type model:

$$\sigma_i(t)+\frac{\tilde{\eta}_i(\dot{\gamma}(t))}{g_i}\dot{\sigma}_i(t)=-\tilde{\eta}_i(\dot{\gamma}(t))\dot{\gamma}(t)$$
$$\sigma(t)=\sum_i \sigma_i(t) \tag{10}$$

Here i = 1, 2, ..., 6 is the element index, σ is the full shear stress, σ_i is the shear stress of the i^{th} element. η_i and g_i are the i^{th} viscosity and elastic modulus parameter of the fitted Maxwell model. The shear rate dependent viscosities $\tilde{\eta}_i(\dot{\gamma}(t))$ are defined as:

$$\tilde{\eta}_i(\dot{\gamma}(t))=\sqrt{\left(\frac{\eta_i}{1+(\lambda_i\dot{\gamma}(t))^2}\right)^2+\left(\frac{\eta_i\lambda_i\dot{\gamma}(t)}{1+(\lambda_i\dot{\gamma}(t))^2}\right)^2} \tag{11}$$

where $\dot{\gamma}$ denotes the shear rate and $\lambda_i = \eta_i/g_i$ is the relaxation time parameters of the i^{th} element. This constitutive equation very accurately accounts for the shear thinning of the silicone oil, as detailed in [19]. The simulations were carried out with the Wolfram Mathematica software, where a "virtual rheometer" was implemented as follows. We set the (arbitrary) shear rate signal and the program computes the raw shear stress signal by solving the constitutive equations numerically. Then, from the input shear rate and output shear stress signals, the program calculates all the quantities to characterize the nonlinear viscoelasticity (G'_n, G''_n, G'_M, G'_L, η'_M, and η'_L).

In order to verify our constitutive Equations 10 and 11, we make an interpolation over the raw data of the input shear rate function obtained from the RheoCompass software, and use this as the input of the "virtual rheometer" program. Then we compare the computed stress signal with the measured raw shear stress data, as shown in Figure 6 for several selected representative angular frequencies and amplitudes, indicated in the plots. For each angular frequency, the plot to the left belongs to the linear amplitude regime and the plot to the right represents a nonlinear case. The simulated data fit very well to the measured raw shear stress signal, even at highly non-sinusoidal input shear rates (ω > 10 rad/s and γ_o > 3.98). Figure 7 shows these results in a more suitable representation, using the normalized elastic and viscous Lissajous-Bodwitch curves. The black curves illustrate the measured data, whereas the red curves are the simulated data. Note that even the negative slope was modeled accurately, at ω = 10 rad/s and γ_o = 10. This way we verified that the constitutive equations (Equation 10 and 11) accurately describe the rheological properties of the AK 1.000.000 silicon oil both in the linear and in the nonlinear regime.

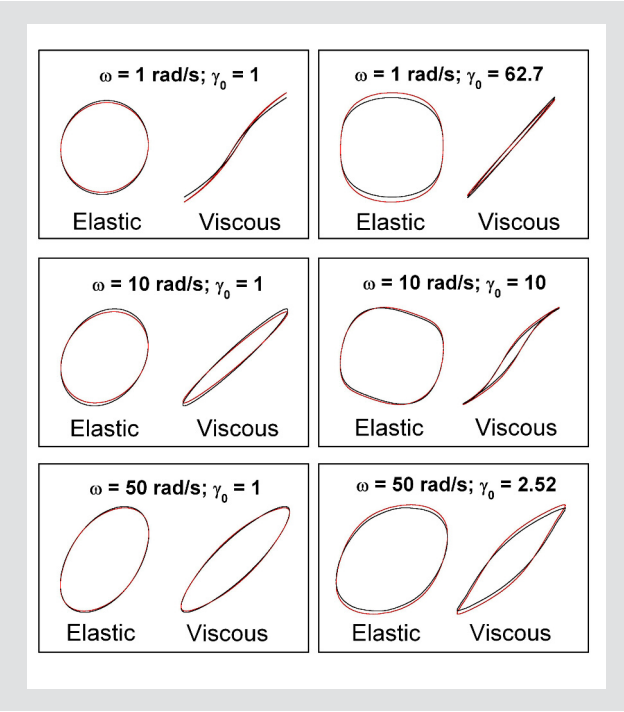

Figure 7: Comparison of the simulated (red) and measured (black) shear stress data shown as elastic and viscous Lissajous-Bodwitch curves for the same parameters as in Figure 6. The plot to the left belongs to the linear amplitude regime and the plot to the right represents a nonlinear case.

6 NONLINEAR VISCOELASTIC PROPERTIES BY EXTENDED LAOS SIMULATIONS

In order to have a more complete LAOS analysis, we extended the parameter range of the LAOS simulations (i.e. the "virtual rheometer" with a strictly sinusoidal shear-rate input) up to ω = 600 rad/s and γ_o = 100. On one hand, we used the result of these simulations to replace the measured data in those cases, where the measurement was not suitable for LAOS analysis for some of the reasons described previously. On the other hand, in the parameter range where we had no measurements at all, we used these simulations for the prediction of the nonlinear viscoelastic features of the silicone oil. It was important to extend the angular frequency range well above the crossover frequency (ω_{CO} = 210 rad/s), in order the give a full LAOS characterization of the silicone oil.

The sine shear-rate controlled LAOS test were simulated for the frequency of ω = 1, 2, 5, 10, 20, 50, 100, 200, 400, and 600 rad/s in a strain amplitude range of γ_o from 0.1 to 100 with 6 points per decade. We present these results with the help of Pipkin diagrams [41], which show the measured data if they were suitable for LAOS analysis, but they show the simulated data otherwise. Figures 8a and 9a show the Pipkin diagrams of the ratios v_3/v_1 and e_3/e_1, respectively where

$$e_1 = G'_1(\omega,\gamma_o), e_3 = -G'_3(\omega,\gamma_o) \tag{12}$$

$$v_1 = G''_1(\omega,\gamma_o), v_3 = G''_3(\omega,\gamma_o) \tag{13}$$

The magnitude of v_3/v_1 characterizes the viscous nonlinearity and that of e_3/e_1 characterizes the elastic nonlinearity. The higher value of the ratio represents higher nonlinearity, because it is actually the ratio of the 3rd harmonic components to the fundamental components, thus these parameters can be easily calculated from the Fourier expansion of the output raw stress signal. Figures 8b and 9b show Pipkin diagrams of T and S, respectively as defined by Equations 4 and 5. The color code shows the gradual buildup of the nonlinear behavior from the yellow to the red area, in 9 steps. In the nonlinear regime, the elastic Pipkin diagrams show intracycle strain stiffening (e_3/e_1 > 0 for S > 0) whereas the viscous Pipkin diagrams show intracycle shear thin-

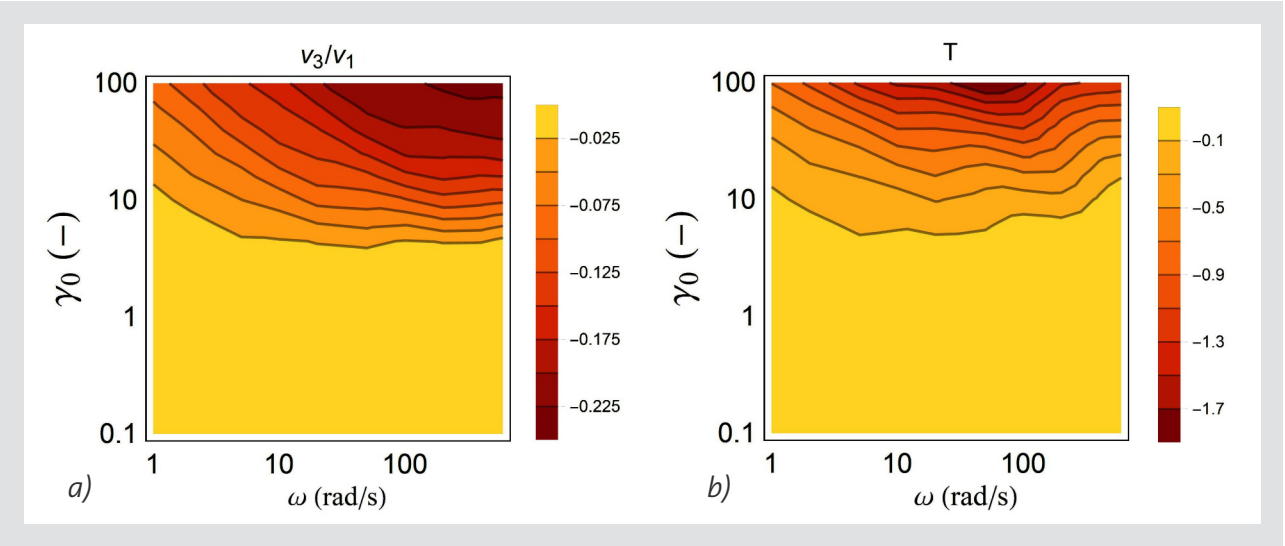

Figure 8: Pipkin diagrams of the v_3/v_1 and the T parameters, which characterize the viscous behavior in LAOS for the combined measured and simulated data as described in the text.

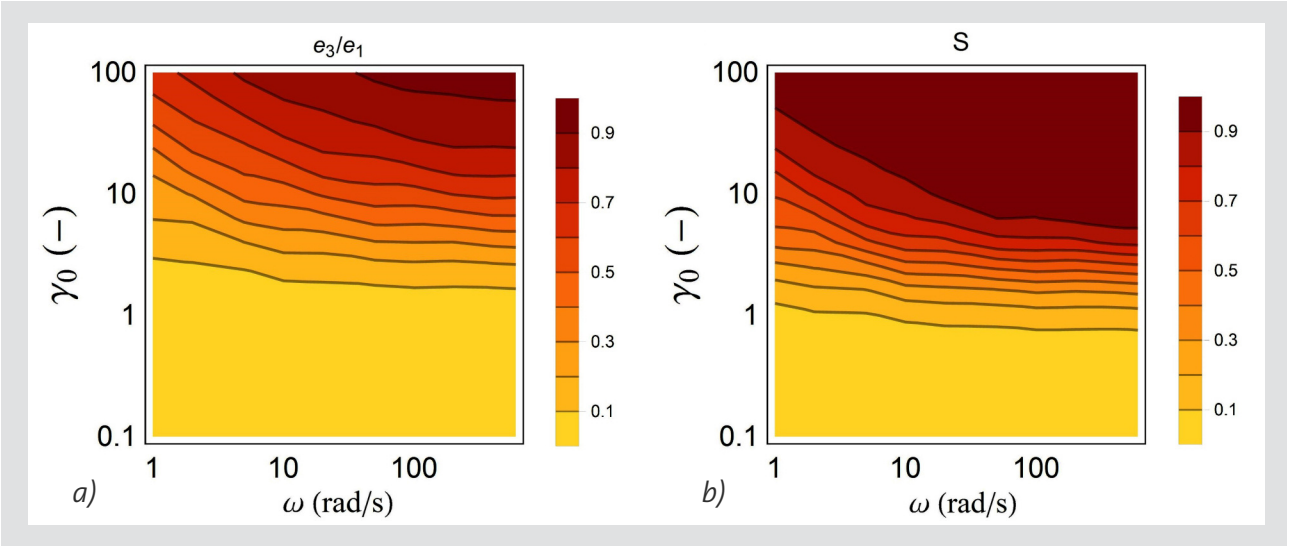

Figure 9: Pipkin diagram of the e_3/e_1 and S parameters, which characterize the elastic behavior in LAOS for the combined measured and simulated data as described in the text.

ning ($v_3/v_1 < 0$ for $T < 0$). At any angular frequency, higher strain amplitude implies higher nonlinearity. The build-up of nonlinear elastic behavior starts at lower strain amplitude and it is much steeper, then that of the nonlinear viscous character. However, taking into account, that the silicone oil is dominantly viscous below ω_{CO} = 210 rad/s, the total viscoelastic stress response can be safely considered linear below strain amplitude 1 and angular frequency 100 rad/s.

Comparing the dependence of the *S* and the *T* parameters on the angular frequency and strain amplitude with that of the e_3/e_1 and the v_3/v_1 ratios, respectively, there are regions with similar structure, but there are also regions with different structure. Since the *S* and *T* parameters include also the effect of the higher-order harmonics, the regions with different structure indicate stronger nonlinearity, where checking only the third harmonic components, i.e. e_3/e_1 and v_3/v_1, is not sufficient to characterize the nonlinear material. Thus, the analysis of *S* in comparison with e_3/e_1 and that of *T* in comparison with v_3/v_1, gives a more complete explanation of the nonlinear viscoelastic properties. Two particular phenomena can be observed from the Pipkin diagrams of *S* and *T*. The *T* parameter has a maximum around ω = 50 rad/s angular frequency. Above ω = 30 rad/s angular frequency the *S* parameter is nearly independent of the angular frequency, so in these cases the material reaches its elastic nonlinearity only due to the strain amplitude.

7 CONCLUSIONS

In this paper, we investigated the nonlinear viscoelastic properties of a high viscosity silicone oil, using LAOS tests performed with a high precision rotational rheo-

meter. Earlier results already have shown that this silicone oil is shear thinning, and both the storage and the loss moduli decrease with increasing oscillation amplitude in an amplitude sweep test. Based on our new LAOS tests, the total viscoelastic stress response can be safely considered linear below strain amplitude 1 and angular frequency 100 rad/s. In the nonlinear regime, the elastic Lissajous-Bodwitch curves show intracycle strain stiffening whereas the viscous Lissajous-Bodwitch curves show intracycle shear thinning. We carefully analyzed also the raw data of our new LAOS tests and discarded from the LAOS analysis those cases where the input shear-rate signal was not sinusoidal sufficiently. However, we successfully utilized these cases as a verification of our nonlinear viscoelastic model, a 6 element White-Metzner type constitutive equation (Equations 9 and 10). The analysis of S in comparison with v_3/v_1 and that of T in comparison with e_3/e_1 gives a more complete explanation of the nonlinear viscoelastic properties.

REFERENCES

[1] Jerschow P: Silicone elastomers, Smithers Rapra Technology (2002)

[2] Ghannam MT, Esmail MN: Rheological properties of poly(dimethylsiloxane), Ind. Eng. Chem. Res. 37 (1998) 1335–1340.

[3] Hadjistamov D: Viscoelastic properties of filled silicone fluids, Appl. Rheol. 3 (1993) 113–119.

[4] Pavlinek V, Saha P, Kitano T, Tanegashima T: Influence of the electric field on the electrorheological behaviour of cellulose suspensions in silicone oils, Appl. Rheol. 9 (1999) 64–68.

[5] Mall-Gleissle SE, Gleissle W, McKinley GH, Buggisch H: The normal stress behaviour of suspensions with viscoelastic matrix fluids, Rheol. Acta 41 (2002) 61–76.

[6] Hadjistamov D: Viscoelastic behavior of disperse systems with silicone oil and different fillers, Appl. Rheol. 12 (2002) 297–302.

[7] Ziegelbaur RS, Caruthers JM: Rheological properties of poly(dimethylsiloxane) filled with fumed silica: I. Hysteresis behaviour, J. Non-Newton Fluid Mech. 17 (1985) 45–68.

[8] Velankar S, Van Puyvelde P, Mewis J, Moldenaers P: Steady-shear rheological properties of model compatibilized blends, J. Rheol. 48 (2004) 725–744.

[9] Ndong RS, Russel WB: Rheology of surface-modified titania nanoparticles dispersed in PDMS melts: The significance of the power law, J. Rheol. 56 (2012) 27–43.

[10] Rolón-Garrido VH, Wagner MH: The damping function in rheology, Rheol. Acta 48 (2009) 245–284.

[11] Raimbault V, Rebière D, Dejous C, Guirardel M, Pistré J, Lachaud JL: High frequency microrheological measurements of PDMS fluids using saw microfluidic system, Sensors and Actuators B 144 (2010) 467–471.

[12] Brandstaetter M: MCR Series: Correct adjustment of the rheometer and measurement of standard samples using RheoPlus, Anton Paar Application Report C92IA005EN-A, (2013)

[13] Kataoka T, Ueda S: Viscosity-molecular weight relationship for polydimethylsiloxane, Polymer Letters 4 (1966) 317–322.

[14] Kissi NE, Piau JM, Attané P, Turrel G: Shear rheometry of polydimethylsiloxanes. Master curves and testing of Gleissle and Yamamoto relations, Rheol. Acta 32 (1993) 293–310.

[15] Hadjistamov D: Dependance of the first normal stress difference of silicone oils on zero-shear viscosity and molecular weight, Appl. Rheol. 6 (1996) 203–208.

[16] Hadjistamov D: Determination of the onset of shear thinning of polydimethylsiloxane, J. Applied Polymer Sci. 108 (2008) 2356–2364.

[17] Fan Y, Liao H: Experimental studies on the relaxation behavior of commercial polymer melts, J. Applied Polymer Sci. 110 (2008) 1520–1530.

[18] Longin PY, Verdier C, Piau M: Dynamic shear rheology of high molecular weight polydimethylsiloxanes: comparison of rheometry and ultrasound, J. Non-Newton Fluid Mech. 76 (1998) 213–232.

[19] Kokuti Z, Gruijthuijsen van K, Jenei M, Toth-Molnar G, Czirjak A, Kokavecz J, Ailer P, Palkovics L, Völker AC, Szabó G: High-frequency rheology of a high viscosity silicone oil using diffusing wave spectroscopy, Appl. Rheol. 24 (2014) 63984 .

[20] Giacomin AJ, Dealy JM: Large-amplitude oscillatory shear. In: Collyer AA (ed.) Techniques in rheological measurements, Ch 4. Elsevier, London (1993)

[21] Wilhelm M: Fourier-transform rheology, Macromol. Mater. Eng. 287 (2002) 83–105.

[22] Dealy JM, Wissbrun KF: Melt Rheology and its role in plastics processing: Theory and applications, Van Nostrand Reinhold, New York (1990)

[23] Bird RB, Armstrong RC, Hassager O: Dynamics of polymeric liquids [Volume 1: Fluid Mechanics], Wiley, New York (1987).

[24] Cho KS, Hyun K, Ahn KH, Lee SJ: A geometrical interpretation of large amplitude oscillatory shear response, J. Rheol 49 (2005) 747–758.

[25] Ewoldt RH, Clasen C, Hosoi AE, McKinley GH: Rheological fingerprinting of gastropod pedal mucus and synthetic complex fluids for biomimicking adhesive locomotion, Soft Matter 3 (2007) 634–643.

[26] Hyun K, Nam JG, Wilhelm M, Ahn KH, Lee SJ: Large amplitude oscillatory shear behaviour of PEO-PPO-PEO triblock copolymer solutions, Rheol. Acta 45 (2006) 239–249.

[27] Philippoff W: Vibrational measurements with large amplitudes, Trans Soc. Rheol. 10 (1966) 317–334.

[28] Sim HG, Ahn KH, Lee SJ: Large amplitude oscillatory shear behaviour of complex fluids investigated by a network model: a guideline for classification, J Non-Newton Fluid Mech 112 (2003) 237–250.

[29] Tee TT, Dealy JM: Nonlinear viscoelasticity of polymer melts, Trans Soc Rheol 19 (1975) 595–615.

[30] Carotenuto C, Grosso M, Maffettone PL: Fourier transform rheology of dilute immiscible polymer blends: A novel procedure to probe blend morphology, Macromolecules 41 (2008) 4492–4500.

[31] Klein CO, Spiess HW, Calin A, Balan C, Wilhelm M: Separation of the nonlinear oscillatory response into a superpo-

sition of linear, strain hardening, strain softening, and wall slip response, Macromolecules 40 (2007) 4250 – 4259.
[32] Neidhöfer T, Sioula S, Hadjichristidis N, Wilhelm M: Distinguish linear from star-branched polystyrene solutions with Fourier-transform rheology, Macromol. Rapid Commun. 25 (2004) 1921 – 1926.
[33] Fleury G, Schlatter G, Muller R: Non linear rheology for long chain branching characterization, comparison of two methodologies: Fourier transform rheology and relaxation, Rheol. Acta 44 (2004) 174 – 187.
[34] Schlatter G, Fleury G, Muller R: Fourier transform rheology of branched polyethylene: Experiments and models for assessing the macromolecular architecture, Macromolecules 38 (2005) 6492 – 6503.
[35] Vittorias I, Parkinson M, Klimke K, Debbaut B, Wilhelm M: Detection and quantification of industrial polyethylene branching topologies via Fourier-transform rheology, NMR and simulation using the Pom-pom model, Rheol. Acta 46 (2007) 321 – 340.
[36] Hyun K, Ahn KH, Lee SJ, Sugimoto M, Koyama K: Degree of branching of polypropylene measured from Fourier-transform rheology, Rheol. Acta 46 (2006) 123 – 129.
[37] Hyun K, Baik ES, Ahn KH, Lee SJ, Sugimoto M, Koyama K: Fourier-transform rheology under medium amplitude oscillatory shear for linear and branched polymer melts, J. Rheol. 51 (2007) 1319 – 1342.
[38] Ewoldt RH, Hosoi AE, McKinley GH: New measures for characterizing nonlinear viscoelasticity in large amplitude oscillatory shear, J. Rheol. 52 (2008) 1427 – 1458.
[39] Läuger J, Stettin H: Differences between stress and strain control in the non-linear behavior of complex fluids, Rheol. Acta 49 (2010) 909 – 930.
[40] Hyun K, Wilhelm M, Klein CO, Cho KS, Nam JG, Ahn KH, Lee SJ, Ewoldt RH, McKinley GH: A review of nonlinear oscillatory shear tests: Analysis and application of large amplitude oscillatory shear (LAOS), Progress in Polymer Sci. 36 (2011) 1697 – 1753.
[41] Pipkin AC: Lectures on viscoelasticity theory, Springer, New York (1972).